Dalton Transactions

ROYAL SOCIETY OF CHEMISTRY

PAPER

View Article Online
View Journal | View Issue

Cite this: *Dalton Trans.*, 2021, **50**, 17062

Multiferroic Aurivillius $Bi_4Ti_{2-x}Mn_xFe_{0.5}Nb_{0.5}O_{12}$ (n = 3) compounds with tailored magnetic interactions†

Miguel Algueró, *[a] Jorge Sanz-Mateo,[a] Rafael P. del Real,[a,b] Jesús Ricote,[a] Carmen M. Fernández-Posada[c] and Alicia Castro[a]

Aurivillius compounds with the general formula $(Bi_2O_2)(A_{n-1}B_nO_{3n+1})$ are a highly topical family of functional layered oxides currently under investigation for room-temperature multiferroism. A chemical design strategy is the incorporation of magnetically active $BiMO_3$ units (M: Fe^{3+}, Mn^{3+}, Co^{3+} ...) into the pseudo-perovskite layer of known ferroelectrics like $Bi_4Ti_3O_{12}$, introducing additional oxygen octahedra. Alternatively, one can try to directly substitute magnetic species for Ti^{4+} in the perovskite slab. Previous reports explored the introduction of the M^{3+} species, which required the simultaneous incorporation of a 5+ cation, as for the $Bi_4Ti_{3-2x}Nb_xFe_xO_{12}$ system. A larger magnetic fraction might be attained if Ti^{4+} is substituted with Mn^{4+}, though it has been argued that the small ionic radius prevents its incorporation into the pseudo-perovskite layer. We report here the mechanosynthesis of Aurivillius $Bi_4Ti_{2-x}Mn_xNb_{0.5}Fe_{0.5}O_{12}$ (n = 3) compounds with increasing Mn^{4+} content up to x = 0.5, which corresponds to a magnetic fraction of 1/3 at the B-site surpassing the threshold for percolation, and equal amounts of Mn^{4+} and Fe^{3+}. The appearance of ferromagnetic superexchange interactions and magnetic ordering was anticipated and is shown for phases with $x \geq 0.3$. Ceramic processing was accomplished by spark plasma sintering, which enabled electrical measurements that demonstrated ferroelectricity for all Mn^{4+}-containing Aurivillius compounds. This is a new family of layered oxides and a promising alternative single-phase approach for multiferroism.

Received 5th July 2021,
Accepted 22nd October 2021

DOI: 10.1039/d1dt02220b

rsc.li/dalton

1. Introduction

Magnetoelectric multiferroics are compounds that show the coexistence of ferroelectricity and magnetic order.[1,2] They can present comparatively large magnetoelectric coefficients[2] and coupled ferroelectric and magnetic domains.[3] This opens the possibility of obtaining electrically driven magnetization reversal, which is the key to developing magnetoelectric memory devices combining low-power, fast electrical-writing with non-destructive magnetic reading.[4] This is only one example out of a wide range of related technologies that would make use of the ability to control electric polarization with a magnetic field and conversely of magnetization with an electric field.[5,6] However, despite extensive research, compounds capable of enabling these technologies have not been developed yet, and the design of material single-phase approaches that result in the required functional magnetoelectric responses remains a challenge.[7] The main issue is that essentially all spin-driven multiferroics only develop ordering below room temperature (RT)[8] and that the few examples of type I compounds, *i.e.* with independently developed ferroic orders, and multiferroic at RT are mostly $BiFeO_3$-based materials with weak ferromagnetism.[9–11]

A very active line of research concentrates on Aurivillius phases. These layered oxide compounds of the general formula $M_2A_{n-1}B_nO_{3n+3}$ consist of alternating $[M_2O_2]^{2+}$ and perovskite-like $[A_{n-1}B_nO_{3n+1}]^{2-}$ blocks, where n is the number of octahedral units in the pseudo-perovskite layer and M is generally Bi^{3+},[12,13] but for a few examples that have other lone-pair containing (ns^2) species at the M-site.[14–16] The Aurivillius family displays high chemical flexibility, and different large cations like Bi itself, lanthanides and group II metals can occupy the A-site, while smaller d^0 transition metals like Ti^{4+}, Nb^{5+} and W^{6+} generally occupy the B-site.[17] A number of compounds are ferroelectric and are being used in non-volatile random access memory and as high-temperature

[a]*Instituto de Ciencia de Materiales de Madrid (ICMM), CSIC, Cantoblanco, 28049 Madrid, Spain. E-mail: malguero@icmm.csic.es*
[b]*Instituto de Magnetismo Aplicado (UCM), Unidad Asociada (CSIC), Spain*
[c]*Maxwell Centre, Cavendish Laboratory, University of Cambridge, Cambridge CB3 0HE, UK*

†Electronic supplementary information (ESI) available. See DOI: 10.1039/d1dt02220b

piezoelectrics.[18,19] The possibility of achieving multiferroism by incorporating magnetically active cations into the B-site of a pseudoperovskite layer is being actively investigated and several room temperature multiferroics,[20–24] along with magnetoelectric coupling[23,25] and even magnetic driving of ferroelectric domains,[21–23] have already been demonstrated.

Most activity concentrates in $[Bi_2O_2][Bi_{2+m}Ti_3Fe_mO_{10+3m}]$ compounds. The chemical design strategy behind this series is the addition of m units of magnetically active $BiFeO_3$ to the pseudo-perovskite layer of the well-known ferroelectric $Bi_4Ti_3O_{12}$, increasing in this way the number of oxygen octahedra n. $Bi_5Ti_3FeO_{15}$ with $n = 4$ is obtained after the addition of one $BiFeO_3$, which is ferroelectric and develops magnetic order at 80 K.[26] Short-range superexchange interactions are the dominant coupling mechanisms between magnetic cations in insulating oxides and are antiferromagnetic for these Aurivillius compounds.[26,27] Percolation of the magnetic species at the B-site sublattice, *i.e.* each magnetic species having at least one magnetic nearest neighbor, is assumed necessary for obtaining long-range order. However, this is not attained for $Bi_5Ti_3FeO_{15}$, whose magnetic fraction at the B-site is clearly below the minimal average occupation of a simple cubic lattice for percolation (0.312).[28] This threshold is surpassed by the addition of a second $BiFeO_3$ to obtain $Bi_6Ti_3Fe_2O_{18}$ and the magnetic fraction continuously increases along the $Bi_{4+m}Ti_3Fe_mO_{12+3m}$ series as m and thus n increase. All $Bi_6Ti_3Fe_2O_{18}$, $Bi_7Ti_3Fe_3O_{21}$, $Bi_8Ti_3Fe_4O_{24}$ and $Bi_9Ti_3Fe_5O_{27}$ phases have been prepared and shown to be antiferromagnetic with increasing Néel temperature.[26,29–31] Nonetheless, the preparation becomes increasingly difficult with the increase of n and random intergrowths of low-n phases are often obtained.[32] Several reports of room temperature weak ferromagnetism have been published and are related to the presence of magnetic clustering.[33] However, the magnetization values are usually of only several memu g^{-1} and such signals can easily be caused by traces of magnetic impurities below the sensitivity of X-ray powder diffraction techniques.[34]

An alternative design approach for obtaining magnetic order starting from $Bi_4Ti_3O_{12}$ is to directly substitute magnetic species for Ti^{4+} at the B-site of the perovskite layer, without increasing the number of octahedral units. This has been done by substituting Fe^{3+} for Ti^{4+} in the ferroelectric $n = 3$ phase, which required the simultaneous incorporation of a 5+ cation like Nb or Ta to maintain charge neutrality.[35] A recent work explored the synthesis of $Bi_4Ti_{3-2x}Fe_xNb_xO_{12}$ compounds with high x surpassing the percolation threshold and succeeded in obtaining $Bi_4TiFeNbO_{12}$ that showed room temperature magnetic order, along with ferroelectricity.[24]

An issue common to all these multiferroic layered oxides is that the attained room-temperature magnetization values are consistently low. Significantly higher magnetization values were obtained when Fe^{3+} was partially replaced with Co^{3+}, either in the $n = 3$ phase[23] or the $n = 4$ and 5 phases.[22,36,37] Indeed, a saturation magnetization of 1.85 emu g^{-1} was recently reported for $Bi_{5.25}La_{0.75}Ti_3FeCoO_{18}$.[37] Random intergrowths of different n-value phases are promoted by Co substitution and local short-range ordered Fe–O–Co clusters at the phase boundaries have been proposed to be responsible for the increased magnetization.[36] Enhanced ferromagnetism has also been obtained after Mn^{3+} substitution and a saturation magnetization of 0.74 emu g^{-1} has been reported for $Bi_6Ti_3Fe_{2-x}Mn_xO_{18}$ sol–gel thin films.[21] Uncontrolled partial oxidation of Mn^{3+} to Mn^{4+} and its substitution for Ti^{4+}, according to the measured composition of $Bi_6Ti_{2.8}Fe_{1.52}Mn_{0.68}O_{18}$, has been proposed to be responsible for the ferromagnetism. Similar effects have been previously described for films of $Bi_7Ti_3Mn_3O_{21}$ grown by pulsed laser deposition on $SrTiO_3$.[38]

Actually, the direct substitution of Mn^{4+} for Ti^{4+} in the Aurivillius structure is an appealing possibility to obtain high magnetic fractions at the B-site because it does not require the simultaneous incorporation of a non-magnetic 5+ cation for charge compensation. Besides, if this is done in a compound already containing Fe^{3+}, then ferromagnetic superexchange Fe^{3+}–O^2–Mn^{4+} interactions are introduced.[21] However, it has been argued that the structure is unable to support significant amounts of Mn^{4+} because of its small ionic radius: 0.53 Å in octahedral coordination.[39] Indeed, it was proposed that the B-site can only accommodate metals with radii between 0.58 (W^{6+}) and 0.645 (Fe^{3+}) Å,[40] and a previous attempt to obtain the Mn^{4+}-containing Aurivillius phase $Bi_2Sr_2Nb_2MnO_{12}$ failed.[41] We report here the successful synthesis of $Bi_4Ti_{2-x}Mn_xFe_{0.5}Nb_{0.5}O_{12}$ compounds with increasing Mn^{4+} content up to $x = 0.5$ by a mechanochemical technique. Ceramic processing was accomplished by spark plasma sintering (SPS), and dense materials suitable for electrical and electromechanical characterization studies were obtained for all the new Aurivillius phases, shown to be ferroelectric. Magnetic measurements were also carried out, and they clearly indicated the appearance of ferromagnetic interactions.

2. Experimental

2.1. Synthesis and ceramic processing

The mechanosynthesis of Aurivillius $Bi_4Ti_{2-x}Mn_xFe_{0.5}Nb_{0.5}O_{12}$ compounds with $x = 0$, 0.1, 0.2, 0.3, 0.4 and 0.5 was achieved by the mechanical treatment of precursors in a high-energy planetary mill. Firstly, stoichiometric mixtures of analytical grade Bi_2O_3 (Sigma-Aldrich, 99.9%), TiO_2 anatase (Cerac, 99.9%), MnO_2 (Merck, 85–90%), Fe_2O_3 (Sigma-Aldrich, 99+%) and Nb_2O_5 (Sigma-Aldrich, 99.9%) were thoroughly ground in an agate mortar and 4 g were placed in an 80 cm^3 tungsten carbide vessel along with five 20 mm diameter balls of the same material for mechanical treatment in a Fritsch Pulverisette 6 mill operating at 300 rpm. These conditions were recently shown to be adequate for the mechanosynthesis of $Bi_4Ti_{3-2x}Fe_xNb_xO_{12}$ compounds up to $x = 1$.[24] Cumulative cycles of 30 min milling and 10 min break were used, which prevented overheating and allowed small amounts of sample to be retrieved for monitoring the mixture evolution. The phases were monitored by X-ray powder diffraction (XRD) with a Bruker AXS D8 Advance diffractometer. Patterns were

recorded between 12 and 60° 2θ, with °2θ increments of 0.05 and a counting time of 0.2 s per step. The Cu-Kα doublet (λ = 1.5418 Å) was used in the measurements. Aurivillius nanocrystalline phases were obtained for all cases, and milling was stopped after 24 h when neither traces of precursors nor secondary phases were observed. Synthesis completion was confirmed by carrying out thermal treatments at increasing temperatures in a conventional furnace, after which no secondary phases appeared until high temperatures when the Aurivillius phase started decomposing. Product morphology was characterized by field emission scanning electron microscopy (FEG-SEM) with a Philips XL 30 S-FEG FE-SEM apparatus.

Ceramic processing of the mechanosynthesized phases was only possible by spark plasma sintering. Experiments were carried out with an SPS-212Lx Dr Sinter Lab Jr. system, with dies of 8 mm diameter and ≈1.2 g of material. Graphite dies and temperatures just below the onset of phase decomposition, as determined in the previous cumulative heating experiments (see Table 1), were initially tested with a pressure of 60 MPa. In a typical five-step process, the temperature was linearly raised up to 100 °C below the target one in 4 min and at the same time the pressure was increased until 50 MPa (I). Secondly, the final temperature and pressure were attained in another 2 min (II) and the system conditions were maintained for 5 min (III). Finally, the temperature was reduced to 300 °C in 2 min while the pressure was reduced to 50 MPa (IV). Full unloading was performed in another minute and at the same time room temperature was reached (V). Note that the full process only lasted 15 min. This is the same protocol used in ref. 24 for the ceramic processing of $Bi_4Ti_{3-2x}Fe_xNb_xO_{12}$, which is also suitable for $Bi_4Ti_{2-x}Mn_xFe_{0.5}Nb_{0.5}O_{12}$. The densification attained was measured after the experiment by Archimedes' method, while the phases were controlled by XRD with the same equipment used to monitor the synthesis. As secondary phases appeared for all phases under the initial conditions, decreasing temperatures were tested until they disappeared while pressure was raised when necessary to obtain high densification (≥95%). For materials with high x-values, namely x = 0.4 and 0.5, tungsten carbide dies were used instead of the graphite ones because the latter dies failed under the required low temperature and high-pressure conditions. Actually, dense materials could not be obtained by spark plasma sintering of the nanocrystalline phase with x = 0.5. This motivated a second set of experiments starting from thermally treated layered oxides, which resulted in dense ceramics free of secondary phases for all cases.

Table 1 Crystal structure evolution: lattice parameters a, b and c, and volume V of the Aurivillius orthorhombic $B2cb$ crystal cell for the $Bi_4Ti_{2-x}Mn_xFe_{0.5}Nb_{0.5}O_{12}$ compounds. Temperatures T of the thermal treatments are indicated

x	T [°C]	a [Å]	b [Å]	c [Å]	V [Å^3]
0	850	5.455(5)	5.444(2)	33.17(2)	985(1)
0.1	800	5.444(2)	5.442(1)	33.219(9)	984.1(5)
0.2	800	5.437(2)	5.4362(8)	33.183(8)	980.8(4)
0.3	800	5.440(2)	5.436(1)	33.13(1)	979.8(6)
0.4	800	5.436(2)	5.435(1)	33.12(1)	978.4(5)
0.5	600	5.428(7)	5.438(3)	33.02(3)	975(2)

2.2. Characterization

The crystallographic symmetry and cell parameters of the obtained Aurivillius phases were characterized by XRD. This was done on samples with enhanced crystallinity prepared by heating the as-mechanosynthesized oxides at the maximum temperature that the compounds withstand before the secondary phases appeared. Patterns in this case were also recorded between 12 and 60° 2θ, with a reduced °2θ increment of 0.02 and an enlarged counting time of 2.7 s per step. The refinements were accomplished using a least-square method (CELREF).

A key aspect of the current study is the actual valence state of Mn, which was determined by X-ray photoelectron spectroscopy (XPS). Measurements were carried out using an Escalab 250XI spectrometer from Thermo Fisher Scientific operating in constant analyser energy mode. A monochromatic Al-K_α source (1486.74 eV), a flood gun for charge compensation and a 900 μm spot size were used. A large enough number of scans were accumulated in the Mn 2p region, using a pass energy of 50 eV, a step size of 0.05 eV, and a dwell time of 50 ms. The position of the adventitious C 1s (binding energy of 284.6 eV for the C–C) was selected to calibrate the energy scale of the spectra. The CASA XPS software was chosen to analyze the spectra, using a Shirley background and GL(60) curve fitting for the Mn 2p signals. The Aurivillius phase with the largest amount of Mn (x = 0.5), along with the MnO_2 precursor as reference were measured.

Ceramic capacitors for electrical characterization were prepared by painting silver electrodes on the opposite faces of the spark plasma sintered discs, followed by firing at 700 °C but for the Aurivillius compound with x = 0.5, which required decreasing the temperature down to 600 °C to avoid phase decomposition. In the first step, the temperature dependences of the dielectric permittivity and losses were measured between room temperature (RT) and the temperature electrodes had been fired with an Agilent E4980A LCR meter. Measurements were dynamically carried out during a heating/cooling cycle with ±1.5 °C min^{-1} rate at several frequencies between 100 Hz and 1 MHz. Secondly, RT high field response was recorded under voltage sine waves of 0.1 Hz frequency and increasing amplitude up to 10 kV, obtained by the combination of an HP 3325B synthesizer/function generator and a TREK 10/40 high-voltage amplifier, while the charge was measured with a homebuilt charge to voltage converter and a software for loop acquisition and analysis. The same equipment was used to obtain resistivity as a function of x by fitting the low field and frequency responses to that of an RC parallel element.

In addition, piezoresponse force microscopy (PFM) experiments were carried out for selected Aurivillus compounds. This is a contact mode scanning probe microscopy for characterizing ferroelectrics based on the measurement of the local

surface deformation under an alternate voltage (converse piezoelectric effect) applied between the tip and the sample. This is done as the tip is scanned to reveal polar domains and at a fixed position as the voltage is increased in steps to obtain piezoresponse hysteresis loops when polarization is locally reversed.[42] The technique can also be used for writing domains, by scanning the tip under a bias field above the coercive one, as determined from the piezoresponse loops. The details of the experimental set-up and protocol for bulk ceramic samples can be found in ref. 43.

The magnetic response was characterized on the SPS discs. Two types of measurements were carried out with a KLATencorEV7a vibrating-sample magnetometer (VSM). Firstly, magnetization was measured between 90 and 400 K under an applied field of 300 Oe, after initial zero field cooling (ZFC) and successive field cooling (FC). Secondly, the isothermal magnetization was measured with fields up to 18 kOe.

Finally, ceramic microstructures were characterized after polishing one surface of the sintered discs with alumina suspensions of decreasing particle size down to 0.1 μm, followed by thermal etching at and quenching from a temperature equal to that attained in the electrical measurements. Note that actual values were above SPS temperatures for $x \geq 0.2$ and thus the occurrence of some additional grain growth cannot be disregarded in these cases. A Philips XL 30 S-FEG FE-SEM apparatus was also used in these studies after metallizing the samples with a Cr coating. Additional experiments were carried out for $x = 0.5$ with a Nova™ NanoSEM 230 microscope equipped with an Oxford INCA 250 energy dispersive X-ray spectrometer (EDXS) in order to control chemical homogeneity.

3. Results and discussion

3.1. Synthesis of the Aurivillius $Bi_4Ti_{2-x}Mn_xFe_{0.5}Nb_{0.5}O_{12}$ compounds

As already anticipated, Aurivillius single-phase nanocrystalline oxides were obtained for all cases up to $x = 0.5$, *i.e.* $Bi_4Ti_{1.5}Mn_{0.5}Fe_{0.5}Nb_{0.5}O_{12}$ that has a magnetic fraction at the B-site of 1/3 and nominally equal mole percentages of Mn^{4+} and Fe^{3+}, by mechanosynthesis. No significant differences in the mixture evolution during mechanical treatment or in the required milling times for completing the synthesis were found among samples. Hence, the addition of MnO_2 to the system did not seem to significantly modify the process. Phase evolution during the milling is illustrated in Fig. 1a for the layered oxide with the largest amount of Mn^{4+} ($x = 0.5$) as an example. Severe particle size reduction takes place during the first hour of mechanical treatment and amorphization has been mostly attained after three hours, yet traces of nanocrystalline precursors are still present. An Aurivillius phase is formed upon further milling and it is basically isolated after 18 h. No further evolution is found when mechanical treatment is prolonged until 24 h, the time at which the reaction is reckoned complete. Powder morphology is shown in the SEM image of Fig. 1b, where submicron-sized tight agglomerates of nanometric primary particles are revealed.

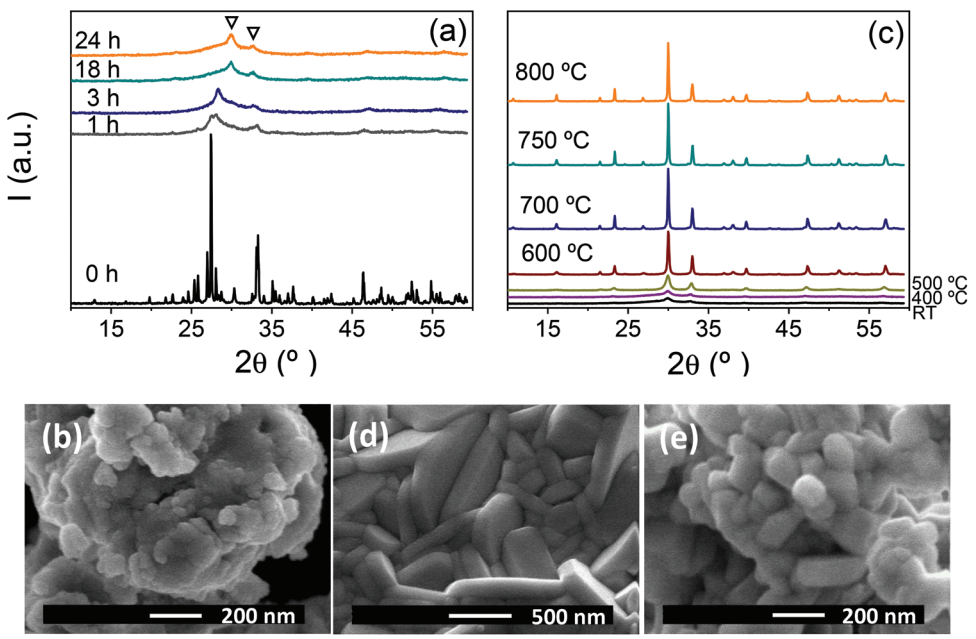

Fig. 1 Mechanosynthesis: XRD patterns of (a) precursors of $Bi_4Ti_{1.5}Mn_{0.5}Fe_{0.5}Nb_{0.5}O_{12}$ ($x = 0.5$) after mechanical treatment for increasing times until the synthesis of the Aurivillius compound (associated peaks indicated with ∇) and (c) the mechanosynthesized $Bi_4Ti_{1.6}Mn_{0.4}Fe_{0.5}Nb_{0.5}O_{12}$ ($x = 0.4$) Aurivillius phase after cumulative thermal treatments at increasing temperatures; morphology of the mechanosynthesized Aurivillius $Bi_4Ti_{2-x}Mn_xFe_{0.5}Nb_{0.5}O_{12}$ compounds with (b) $x = 0.3$, (d) $x = 0.3$ after thermal treatment at 800 °C, and (e) $x = 0.5$ after treatment at 600 °C (SEM images).

Neither residual precursors nor intermediate phases appeared when the nanocrystalline powders were heated at increasing temperatures until the Aurivillius compound decomposed, which confirmed the synthesis completion. The XRD patterns of $Bi_4Ti_{1.6}Mn_{0.4}Fe_{0.5}Nb_{0.5}O_{12}$ (x = 0.4) after cumulative thermal treatments are shown in Fig. 1c as examples. This Aurivillius phase was stable up to 800 °C, the temperature above which secondary phases were found. The maximum temperature that the compounds withstood before decomposing was not the same for all phases but slightly decreased from 850 (x = 0) down to 800 °C after Mn substitution (x = 0.1), stayed constant up to x = 0.4, and dropped down to 600 °C for x = 0.5. The reduced thermal stability of this latter phase is remarkable.

Particle growth took place during heating and a platelet-like morphology typical of Aurivillius compounds developed. Not surprisingly, dimensions scaled with temperature and thus significantly larger platelets were obtained for phases with x up to 0.4 (a diameter of 0.5–1.5 μm and a thickness of 0.15–0.30 μm) than for that with x = 0.5, whose particles only presented an incipient anisometry and diameters around ~0.1 μm with a significant population still in the nanoscale (see Fig. 1d and e).

3.2. Crystal structure characterization of the Aurivillius $Bi_4Ti_{2-x}Mn_xFe_{0.5}Nb_{0.5}O_{12}$ compounds

The XRD patterns of all Aurivillius compounds are shown in Fig. 2a after a thermal treatment to enhance crystallinity. The temperature of the treatment was the maximum one that could be reached before each phase started decomposing, as stated in the previous section (and given in Table 1). Particle and thus, crystal size was not the same across the series but it was in the submicron range for compounds with x up to 0.4 and decreased down to the nanoscale when x was raised up to 0.5. All patterns can be indexed as an Aurivillius phase with n = 3 and the non-centrosymmetric orthorhombic $B2cb$ space group. This is the same group assigned to all $Bi_4Ti_{3-2x}Fe_xNb_xO_{12}$ phases up to x = 1 (ref. 24) and is also commonly used for powdered samples of $Bi_4Ti_3O_{12}$ (the $B1a1$ space group) when crystallinity is not high enough and monoclinic distortion is not observed in the diffraction patterns.[44,45]

The refined cell parameters for the different phases are given in Table 1, along with the lattice volume that is also shown in Fig. 2b as a function of x. Note the gradual contraction of the crystal lattice, which suggests the formation of an Aurivillius solid solution all across the compositional range investigated. This is the expected behavior according to the ionic radius of Ti^{4+} and Mn^{4+} in octahedral coordination: 0.605 and 0.53 Å, respectively.

One main result of this research thus is the mechanosynthesis of Aurivillius $Bi_4Ti_{2-x}Mn_xFe_{0.5}Nb_{0.5}O_{12}$ compounds incorporating Mn as 4+ up to x = 0.5 that has a magnetic fraction of 1/3 above the threshold for percolation and equal percentages of Mn^{4+} and Fe^{3+}. The superexchange Mn^{4+}–O^{2-}–Fe^{3+} interactions are expected to be ferromagnetic and to be maximized for $Bi_4Ti_{1.5}Mn_{0.5}Fe_{0.5}Nb_{0.5}O_{12}$ (x = 0.5). The 4+ valence for Mn was confirmed by XPS. The spectra across the Mn 2p region are shown in Fig. 3 for the Aurivillius phase with x = 0.5 and the MnO_2 precursor as reference. The peaks could be fit with a single component, whose binding energy values (Mn $2p_{3/2}$ at 642.1 eV and Mn $2p_{1/2}$ at 653.7 eV) agree with those of the Mn^{4+} reference. The presence of significant amounts of Mn^{3+} or Mn^{2+} can then be ruled out.

This is the first report of an Aurivillius phase containing Mn at the 4+ state, which could be only obtained by mechanosynthesis. Mechanochemical techniques are a powerful means of preparing nanocrystalline functional oxides, which have been extensively applied to the preparation of ferroelectric perovskites.[46] In particular, mechanosynthesis in high energy planetary mills has been shown to be suitable for obtaining low tolerance factor perovskites that are metastable at ambient pressure, such as high sensitivity piezoelectric $Pb(Zn_{1/3}Nb_{2/3})O_3$-$PbTiO_3$,[47] Bi-rich compositions of the $BiScO_3$–$PbTiO_3$ binary system,[48] and ferromagnetic $BiMnO_{3+\delta}$.[49] The technique is shown here to be also applicable to obtain

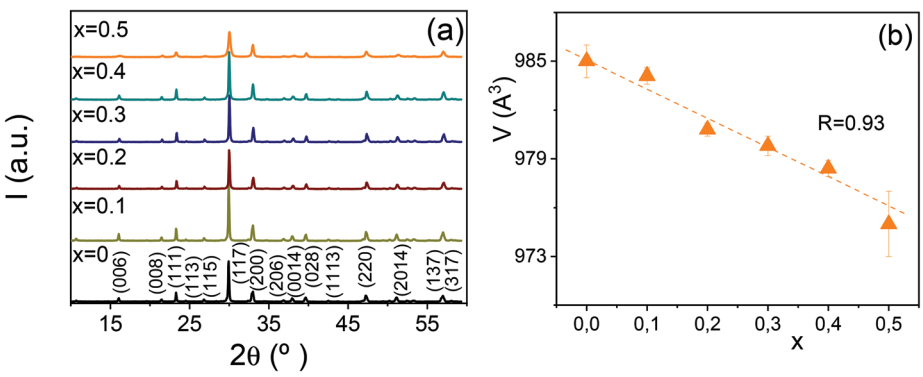

Fig. 2 Crystal structure evolution: (a) XRD patterns of the mechanosynthesized $Bi_4Ti_{2-x}Mn_xFe_{0.5}Nb_{0.5}O_{12}$ compounds after thermal treatment at the maximum temperature they withstand without decomposing (indexation as orthorhombic $B2cb$ is provided: JCPDS no. 35-0795) and (b) lattice volume V as a function of x as obtained from the refined cell parameters assuming the Aurivillius orthorhombic $B2cb$ crystal cell (linear regression factor R is indicated).

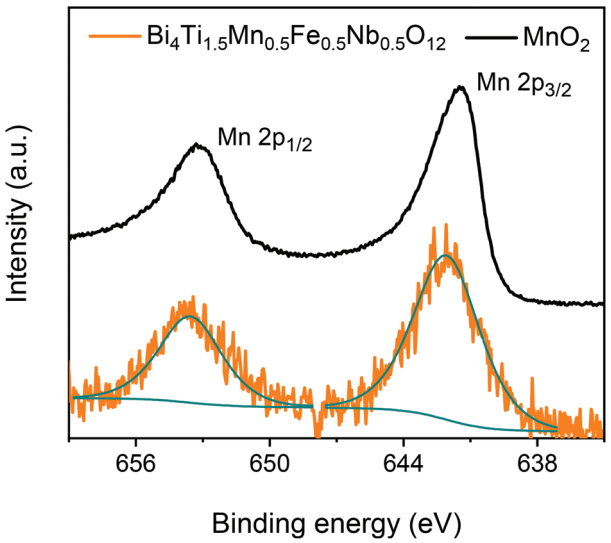

Fig. 3 Mn valence state: XPS spectra for the Aurivillius $Bi_4Ti_{1.5}Mn_{0.5}Fe_{0.5}Nb_{0.5}O_{12}$ compound and the MnO_2 precursor in the energy interval across the Mn 2p region.

Aurivillius compounds incorporating small ionic radius cations like Mn^{4+} at the B-site of the pseudo-perovskite layer.

3.3. Ceramic processing of the Aurivillius $Bi_4Ti_{2-x}Mn_xFe_{0.5}Nb_{0.5}O_{12}$ compounds

Aurivillius single-phase ceramic materials with densifications between 95 and 99% were obtained for all the layered oxides with increasing Mn^{4+} content, when thermally treated phases were used as starting powder for SPS. XRD patterns for the spark plasma sintered ceramics are shown in Fig. 4, which have to be compared with those for the thermally treated powdered phases of Fig. 2a. No differences that might indicate phase changes during the tailored SPS are found and all materials could be consistently indexed as the orthorhombic *B2cb* Aurivillius phase with $n = 3$.

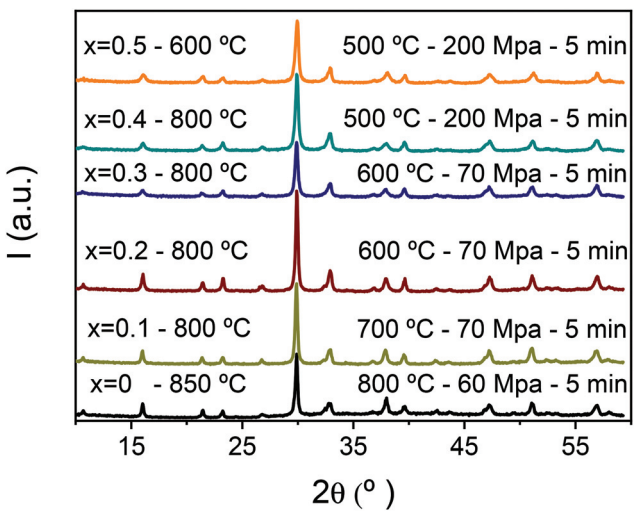

Fig. 4 Processing by spark plasma sintering: XRD patterns of the $Bi_4Ti_{2-x}Mn_xFe_{0.5}Nb_{0.5}O_{12}$ ceramic materials processed from the thermally treated powdered phases (temperature of the powder treatments is indicated next to their composition while the SPS conditions are given in the right side).

The optimized spark plasma sintering conditions for the different compounds are given in Fig. 4. Note that SPS temperatures were systematically lower than those used in the previous thermal treatments of the nanocrystalline phases. This indicates a decreased thermal stability of the Mn^{4+}-containing layered oxides at the reducing conditions involved in the SPS, which is carried out in the presence of graphite and dynamic vacuum. The temperature difference was as high as 300 °C for $x = 0.4$ and not unexpectedly grain growth hardly took place during spark plasma sintering. Indeed, the ability of the SPS technique to fully densify materials with very limited grain growth has been pointed out before and widely used for ceramic nanostructuring.[50,51]

Therefore, the grain size was basically the particle size of the initial powder as indicated by the comparison of the ceramic microstructures provided in Fig. 5a–c with the powder morphology presented in Fig. 1. Ceramic microstructures thus consisted of anisometric grains, typical of Aurivillius phases with an aspect ratio that largely decreased for $x = 0.5$. A submicron grain size resulted for materials up to $x = 0.4$, while a nanoscale grain size was found for $x = 0.5$ that had been processed from phases thermally treated at 600 °C, by SPS at 500 °C and 200 MPa.

No indication of secondary phases was found in the FEG-SEM for any Aurivillius ceramic material as it is illustrated in the ESI† for $x = 0.5$, where additional secondary electron images at reduced magnification are provided (Fig. S1†). Chemical heterogeneities were not found by EDXS and a homogeneous distribution of Bi and B-site cations was revealed by mappings as those shown in Fig. S2.† No significant difference between the average chemical composition and that of individual grains was found and a Bi/B ratio of 1.31 and Ti : Mn : Fe : Nb relations of 1.49 : 0.46 : 0.51 : 0.54 were obtained that are the nominal ones within typical uncertainties of 5–10% for standardless EDXS. Note however that point analysis still averages several grains because of nanostructuring.

The second result of this work is the ceramic processing of all Aurivillius phases, challenging because of their strong tendency to decompose when heated. Recall that the maximum temperature at which the layered oxide with $x = 0.5$ could be thermally treated was as low as 600 °C, even lower than that for the recently reported $Bi_4TiFeNbO_{12}$ (660 °C).[24] Ceramic processing was only possible by the combination of SPS and the highly-sinterable phases obtained by mechanosynthesis, an approach already demonstrated for the stabilization of low tolerance factor perovskites in ceramic form[50,52] and that is shown here to be also suitable for Aurivillius phases with reduced thermal stability. Dense ceramic materials with either submicron ($x \leq 0.4$) or nanometer ($x = 0.5$) size microstructures resulted, which were the key to accomplishing a sound electrical characterization and demonstrating the persistence of ferroelectricity in the Mn^{4+} containing Aurivillius compounds.

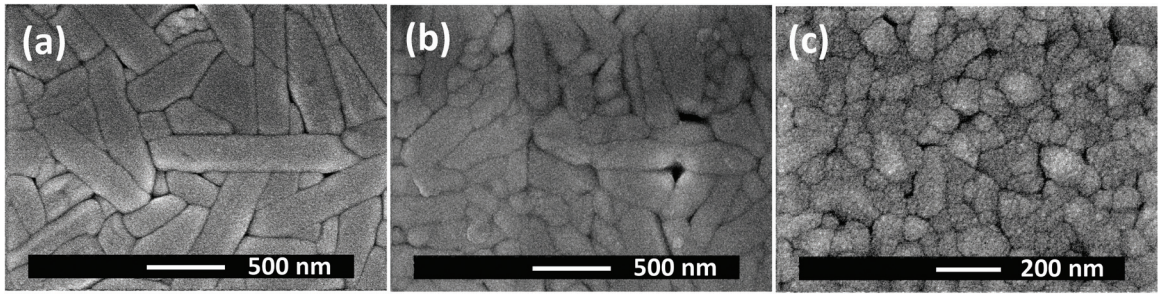

Fig. 5 Processing by spark plasma sintering: microstructure of the Aurivillius $Bi_4Ti_{2-x}Mn_xFe_{0.5}Nb_{0.5}O_{12}$ ceramics with (b) $x = 0$, (c) $x = 0.3$, and (d) $x = 0.5$ (SEM images).

3.4. Electrical characterization of the Aurivillius $Bi_4Ti_{2-x}Mn_xFe_{0.5}Nb_{0.5}O_{12}$ compounds

The temperature and frequency dependences of dielectric permittivity and losses are firstly presented and discussed. The results for $Bi_4Ti_2Fe_{0.5}Nb_{0.5}O_{12}$, whose dielectric properties have already been reported in ref. 24, are given in the ESI (Fig. S3†). This Aurivillius oxide presents a significant dispersion above 100 °C, reflecting the presence of high conductivity, though decreased as compared with $Bi_4Ti_3O_{12}$. This has been shown to be a p-type conductivity, associated with either the compensation of Bi vacancies by holes or the presence of acceptor impurities, and reduced by the Fe^{3+}/Nb^{5+} co-substitution.[24] Like $Bi_4Ti_3O_{12}$, $Bi_4Ti_2Fe_{0.5}Nb_{0.5}O_{12}$ shows two successive dielectric relaxations upon heating before the ferroelectric transition at ≈630 °C, which are present in single crystals[53,54] and ceramics.[55] They have been related to the short range movement of oxygen anions within the crystal lattice,[55] preceding the thermal activation of the ionic conductivity.[56]

The electrical response was deeply modified by the substitution of Mn^{4+} for Ti^{4+}. The results of $Bi_4Ti_{2-x}Mn_xFe_{0.5}Nb_{0.5}O_{12}$ ceramic materials with increasing x are also given in the ESI (Fig. S4†). Dielectric dispersion was largely enhanced, so that it was already significant at room temperature. Indeed, the low frequency permittivity readily increased with x from ≈290 for $x = 0.1$ up to 415 and 1255 for $x = 0.3$ and 0.5, respectively, at 100 Hz and RT. The two relaxations were not observed anymore, and instead a distinctive step-like increase in permittivity appeared, whose height and position decreased and shifted to high temperatures, respectively, with frequency. This is characteristic of a Maxwell–Wagner (M–W) type relaxation, associated with the blocking and accumulation of free charge carriers at interfaces, commonly grain boundaries in the case of ceramic materials.[52,57] The steps of relative permittivity are accompanied by maxima in the loss tangent (see insets in Fig. S4†), though they are partially masked in the $Bi_4Ti_{2-x}Mn_xFe_{0.5}Nb_{0.5}O_{12}$ ceramics by a large conduction background that suggests imperfect blocking at the boundaries. Note the large dielectric losses that exponentially rise with temperature and also increase with Mn^{4+} content as shown in Fig. 6a; imaginary permittivity is proportional to the reciprocal dc conductivity. The rising bulk conductivity is additionally indicated by the increasing height of the M–W relaxation with x, which shifts to low temperatures too. This is the expected behavior when the characteristic conduction length decreases, *i.e.* grain size in ceramics that does decrease with x. The main effect of the Mn^{4+} substitution then is to introduce additional charge carriers and to enhance conductivity, which also results in the appearance of the M–W dielectric relaxation. A detailed study of the conductivity is out of the scope of this work but it is most probably electronic hopping, likely between the Mn^{4+} and Mn^{3+} species associated with the presence of oxygen vacancies, which are promoted by the reducing conditions during SPS. Room temperature resistivity drops from 2×10^9 Ω m for $x = 0$ down to 1.4×10^8, 3.3×10^7 and 3.0×10^6 Ω m for $x = 0.1$, 0.2 and 0.3, respectively. Above this x-value, resistivity saturates at ~1.5×10^6 Ω m as a result of ceramic nanostructuring, reflecting the increasing weight of less conductive grain boundaries.

At temperatures above the M–W relaxation, the dielectric anomaly associated with the ferroelectric transition can be clearly identified for compositions up to $x = 0.3$ (labelled with T_C). Yet, it is only guessed for $x = 0.4$ and 0.5, most probably because of its overlap with the largely enhanced relaxation (see Fig. S4†). Conduction losses decrease when the frequency is increased so that they are minimized at high frequencies. The temperature dependence of dielectric permittivity at 1 MHz is shown in Fig. 6b for all the Mn^{4+}-containing Aurivillius compounds. A distinctive evolution is confirmed between 0.3 and 0.4 such that sharp dielectric anomalies similar to that of $Bi_4Ti_2Fe_{0.5}Nb_{0.5}O_{12}$ are obtained for $x \leq 0.3$, while markedly increased and broadened ones are found for $x = 0.4$ and 0.5. Nonetheless, when the position of the dielectric anomalies is represented as a function of x, a linear decrease is obtained across the whole x-range investigated (Fig. 6c). This supports all of them to be associated with the ferroelectric transition, also for $x = 0.4$ and 0.5. Note the good correlation between the evolution of Curie temperatures with x and that of lattice volume (Fig. 2b), which is the expected behavior for a ferroelectric solid solution.

Room-temperature high field characterization, aimed at obtaining ferroelectric hysteresis loops, was also carried out but ferroelectric switching was not observed for any material. In the case of $Bi_4Ti_2Fe_{0.5}Nb_{0.5}O_{12}$, the issue was a coercive field

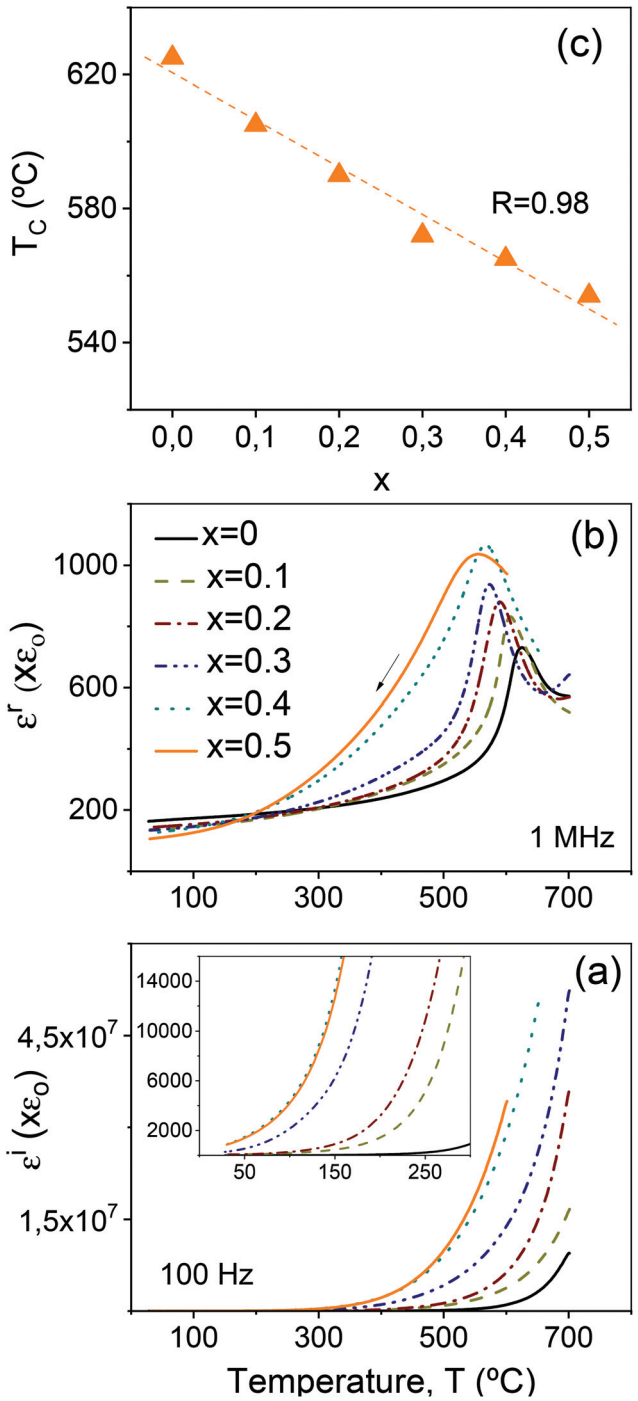

Fig. 6 Dielectric response: temperature dependence of the (a) imaginary permittivity ε^i and (b) real permittivity ε^r for the $Bi_4Ti_{2-x}Mn_xFe_{0.5}Nb_{0.5}O_{12}$ ceramics processed by SPS of thermally treated powdered phases at one selected frequency. (c) Curie temperature T_C, as a function of x, as obtained from the position of the dielectric anomalies in (b). Linear regression factor R is indicated.

that was above 9.5 kV mm^{-1}. This compound showed an effective permittivity that linearly increased with the field, *i.e.* a Rayleigh-type behavior characteristic of ferroelectric materials in the subcoercive regime.[58] In the case of the Mn^{4+}-containing Aurivillius compounds, the problem was the increasing conductivity, which is well known to prevent any ferroelectric characterization. The results for different materials are given in the ESI (Fig. S5†).

The macroscopic electrical characterization then did not demonstrate ferroelectricity, even if an Aurivillius solid solution with the orthorhombic *B2cb* space group, *i.e.* polar was indicated by the structural characterization up to $x = 0.5$, and a dielectric anomaly associated with the ferroelectric transition for $x = 0$ could be followed as x was increased until the same composition. Local ferroelectricity at the microcrystal level was demonstrated for the Aurivillius compound with $x = 0.5$ by piezoresponse force microscopy. Indeed, PFM readily showed the ceramic material to be piezoactive and revealed the polar domains (see Fig. 7a and Fig. S6 in the ESI†). Moreover, local piezoresponse switching could be attained, yet quite large bias voltages were required, and stable ferroelectric domains were reproducibly written and reversed as illustrated in Fig. 7b and c. These results unambiguously demonstrate ferroelectricity until $x = 0.5$ in good agreement with the structural and dielectric characterization studies.

3.5. Magnetic characterization of the Aurivillius $Bi_4Ti_{2-x}Mn_xFe_{0.5}Nb_{0.5}O_{12}$ compounds

The ZFC reciprocal magnetization curves for the $Bi_4Ti_{2-x}Mn_xFe_{0.5}Nb_{0.5}O_{12}$ ceramic materials with increasing Mn^{4+} content are given in Fig. 8a from 90 K to 400 K. The results for $x = 0$ have been previously reported in ref. 24 and showed the presence of a high temperature paramagnetic regime whose extrapolated reciprocal magnetization became zero at a negative temperature, and a deviation from this behavior below ~175 K with the development of an additional magnetization component. A Curie–Weiss analysis between 200 and 400 K provides an effective paramagnetic moment of $5.63\mu_B$ and a C–W temperature of −142 K. This magnetic moment is the average of the individual magnetic cations and has to be compared with a spin-only value of $5.92\mu_B$ for Fe^{3+}. The discrepancy might indicate the presence of some Fe^{2+} (spin-only moment of $4.90\mu_B$) related to the introduction of oxygen vacancies during the spark plasma sintering. The negative C–W temperature confirms antiferromagnetic interactions.

Analogous behaviors were found for $x = 0.1$ and 0.2 with increasing magnetization, as expected from their magnetic fractions. C–W fits were also carried out for these cases. The value for $x = 0.1$ ($5.65\mu_B$) is very close to that expected, averaged from the spin-only moments of Fe^{3+} and Mn^{4+} ($5.58\mu_B$ taking $3.87\mu_B$ for Mn^{4+}). A slight difference could indicate a change in the chemical species compensating for the oxygen vacancies, that is Mn^{3+} (spin-only moment of $4.90\mu_B$) replacing Fe^{2+}. However, the value for $x = 0.2$ ($5.22\mu_B$), though also close to the expected one ($5.33\mu_B$), is below the latter in this case suggesting the opposite trend. Therefore, it seems more sensible to assume the small differences to be associated with errors from the C–W fits, known to be very sensitive to the temperature interval considered. One can then say that the C–

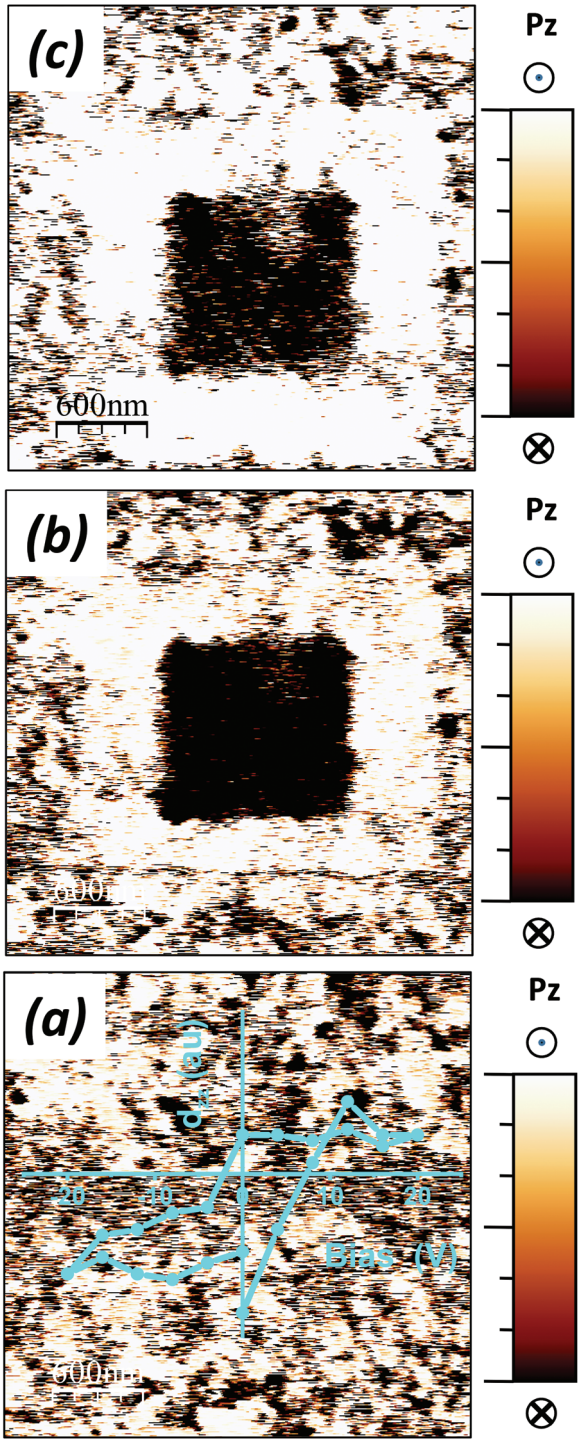

Fig. 7 PFM for $Bi_4Ti_{1.5}Mn_{0.5}Fe_{0.5}Nb_{0.5}O_{12}$: (a) phase image showing the polar domains and the local piezoresponse hysteresis loop. Phase images of (b) an area where ferroelectric domains of opposite directions were successively written (10 V) and (c) the same area after 35 min demonstrating retention.

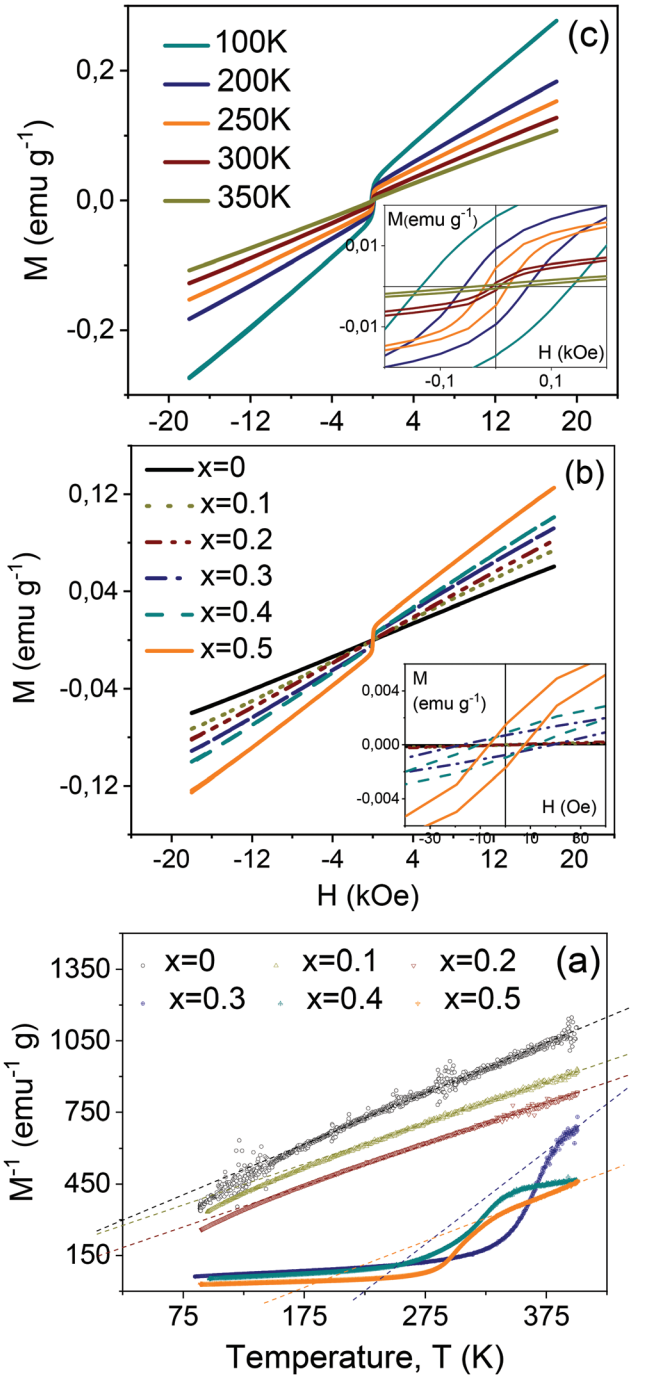

Fig. 8 Magnetic response: (a) ZFC reciprocal magnetizations at 300 Oe and increasing temperatures for the $Bi_4Ti_{2-x}Mn_xFe_{0.5}Nb_{0.5}O_{12}$ ceramics processed by SPS of thermally treated powdered phases; high field isothermal magnetizations for the $Bi_4Ti_{2-x}Mn_xFe_{0.5}Nb_{0.5}O_{12}$ ceramic material with: (b) increasing x at RT and (c) $x = 0.5$ on cooling.

W analyses confirm the 4+ valence state of manganese, yet it must be recalled that Mn substitution causes a significant decrease of resistivity and thus some minor amount of Mn^{3+} is likely present. Regarding C–W temperatures, values of −147 and −102 K are obtained indicating antiferromagnetic interactions to be still dominant. RT response up to 18 kOe is shown in Fig. 8b for all ceramic materials. A very linear magnetization with no hint of hysteresis was found for $x = 0$, 0.1 and 0.2 in agreement with them being room temperature paramag-

nets. The appearance of irreversibility on cooling is illustrated in the ESI† (FC and ZFC curves provided in Fig. S7†) for x = 0.2, along with low temperature weak ferromagnetism.

Magnetic response is drastically modified for the Auriviliius phases with $x \geq 0.3$. Magnetization at 90 K distinctively increased for the compound with x = 0.3 as compared with those with lower x-values. Its evolution on heating was also different so that the reciprocal magnetization showed a step-like increase from ≈325 K that is representative of ferromagnetic interactions. Similar behaviors were found for the x = 0.4 and 0.5 compounds with increasing low temperature magnetizations. In relation to the RT high field response, a distinctive hysteresis was present for x = 0.3, 0.4 and 0.5 supporting their ferromagnetic character with ordering temperatures above room temperature. Remanent magnetizations of 0.68, 0.85 and 1.15 × 10^{-3} emu g^{-1} were obtained for x = 0.3, 0.4 and 0.5, while the coercive field decreased from 18 Oe down to 11 and 7.5 Oe with increasing x. The hysteresis loops at decreasing temperatures are provided in Fig. 8c for the Aurivillius compound with the largest amount of Mn^{4+} (x = 0.5). As typically observed for ferromagnets, both remanent magnetization and coercive field increased upon cooling, up to values of 17 × 10^{-3} emu g^{-1} and 128 Oe, respectively, at 100 K. It is remarkable the lack of saturation for all loops up to fields as high as 18 kOe that indicates a large paramagnetic contribution, and suggests an antiferromagnetic component that would develop at low temperature (Néel temperature below 90 K). The coexistence of ferro- and antiferromagnetic ordering then most probably takes place for $x \geq 0.3$ at low temperatures, which might be associated with magnetic cation partitioning. A distinctive preference of Mn for the central octahedra layers of the perovskite-like block has been proposed for $Bi_2Sr_{1.4}La_{0.6}Nb_2MnO_{12}$ (n = 3)[41] and directly observed for $Bi_6Ti_xFe_yMn_zO_{18}$ (n = 5).[59] Nevertheless, the positive value of the zero reciprocal magnetization extrapolation for x = 0.5 indicates the ferromagnetic response to be dominant for this composition.

Therefore, the results indicate a distinctive evolution of magnetism across the Aurivillius $Bi_4Ti_{2-x}Mn_xFe_{0.5}Nb_{0.5}O_{12}$ solid solution, so that a room temperature ferromagnetic component develops when the amount of Mn^{4+} substituting for Ti^{4+} reaches an x-value of 0.3. Indeed, this was the targeted effect, chemically engineered by the introduction of ferromagnetic superexchange Fe^{3+}–O^{2-}–Mn^{4+} interactions until they outplayed the initial antiferromagnetic Fe^{3+}–O^{2-}–Fe^{3+} ones. The number of Fe^{3+}–O^{2-}–Mn^{4+} bonds is maximized for x = 0.5 which also has the largest magnetic fraction at the B-site, already above the percolation threshold that is only surpassed for this x-value. It was then somehow unexpected that the apparent ordering temperature decreased when x was increased from x = 0.3 up to 0.5. This might be an effect of nanostructuring, for grain size was not constant across the Aurivillius solid solution, but decreased above x = 0.3 down to the nanoscale for x = 0.5. However, the evolution of magnetism between x = 0.2 and 0.3 occurs at constant size in the submicron range.

Nonetheless, a possible effect of magnetic second phase impurities at trace levels must be considered before ferromagnetism can be ascribed to the Mn^{4+}-containing Aurivillius oxides. Indeed, a weight fraction of spinel Fe_3O_4 as small as ~0.00085 could account for the remnant magnetization at 100 K in x = 0.5. In ref. 21, Keeney *et al.* carried out a statistical analysis of a large number of HR-SEM and TEM images at different magnifications for an Aurivillius $Bi_6Ti_{2.8}Fe_{1.52}Mn_{0.68}O_{18}$ material, which showed no Fe_3O_4 and concluded that contribution to remanence from hypothetical unobserved inclusions would be <0.0028 emu g^{-1} with a confidence level above 99.5%. A value of 0.017 emu g^{-1} was obtained for $Bi_4Ti_{1.5}Mn_{0.5}Fe_{0.5}Nb_{0.5}O_{12}$ for which no secondary phases were detected by XRD or FEG-SEM/EDXS. Besides, the continuous evolution of the lattice volume and ferroelectric transition temperature with x, along with that of magnetism clearly indicates the correct substitution of Mn^{4+} for Ti^{4+} in the pseudo-perovskite layer, also confirmed with XPS. Increasing ferromagnetic superexchange interactions and magnetic ordering upon approaching the percolation threshold were expected and have been observed for $x \geq 0.3$.

4. Conclusions

Mechanical treatment in high energy planetary mills is shown to be capable of mechanosynthesizing nanocrystalline Aurivillius $Bi_4Ti_{2-x}Mn_xFe_{0.5}Nb_{0.5}O_{12}$ phases with increasing x-values up to 0.5, which corresponds to a magnetic fraction at the B-site of 1/3, already surpassing the threshold for percolation. This is the first report of an Aurivillius series containing increasing amounts of Mn in the 4+ state, whose ionic radius in octahedral coordination has been previously argued to be too small for its incorporation into the crystal structure. This is attained by the substitution of Ti^{4+} in a three-layer compound containing an Fe^{3+} fraction of 1/6 at the B-site, so that equal percentages of Mn^{4+} and Fe^{3+} are finally obtained. The appearance of ferromagnetic superexchange Mn^{4+}–O^{2-}–Fe^{3+} interactions was anticipated and actually found from x = 0.3, for which room temperature magnetic ordering was also observed.

The Mn^{4+}-containing Aurivillius compounds are unstable under moderate heating, and ceramic processing was only possible by tailored spark plasma sintering of thermally treated phases. Low temperature, high pressure conditions were required above x = 0.3, so that dense materials with decreasing grain size from the submicron range down to the nanoscale were obtained. Macroscopic electrical measurements and local characterization by piezoresponse force microscopy demonstrated ferroelectricity with a high transition temperature that linearly decreased with x. This is in agreement with the evolution of the lattice volume and supports the formation of an Aurivillius ferroelectric solid solution up to x = 0.5, across which tailored magnetic interactions have been engineered.

Conflicts of interest

There are no conflicts to declare.

Acknowledgements

This research was funded by Spanish MICINN through the project MAT2017-88788-R. The XPS system at Cambridge is part of the Sir Henry Royce Institute – Cambridge Equipment, EPSRC grant EP/P024947/1. Technical support by Ms I. Martínez, at ICMM-CSIC is also acknowledged.

Notes and references

1 N. A. Spaldin and M. Fiebig, The renaissance of magnetoelectric multiferroics, *Science*, 2005, **309**, 391–392.
2 W. Eerenstein, N. D. Mathur and J. F. Scott, Multiferroic and magnetoelectric materials, *Nature*, 2006, **442**, 759–765.
3 T. Zhao, A. Scholl, F. Zavaliche, K. Lee, M. Barry, A. Doran, M. P. Cruz, Y. H. Chu, C. Ederer, N. A. Spaldin, R. R. Das, D. M. Kim, S. H. Baek, C. B. Eom and R. Ramesh, Electrical control of antiferromagnetic domains in multiferroic $BiFeO_3$ films at room temperature, *Nat. Mater.*, 2006, **5**, 823–829.
4 M. Bibes and A. Barthelemy, Multiferroics: Towards a magnetoelectric memory, *Nat. Mater.*, 2009, **7**, 425–426.
5 S. Fusil, V. Garcia, A. Barthelemy and M. Bibes, Magnetoelectric devices for spintronics, *Annu. Rev. Mater. Res.*, 2014, **4**, 91–116.
6 G. Dong, Z. Zhou, X. Zue, Y. Zhang, B. Peng, M. Guan, S. Zhao, Z. Hu, W. Ren and Z. G. Ye, Ferroelectric phase transition induced a large FMR tuning in self-assembled $BaTiO_3$:$Y_3Fe_5O_{12}$ multiferroic composites, *ACS Appl. Mater. Interfaces*, 2017, **9**, 30733–30740.
7 N. A. Spaldin and R. Ramesh, Advances in magnetoelectric multiferroics, *Nat. Mater.*, 2019, **18**, 203–212.
8 Y. Tokura, S. Seki and N. Nagaosa, Multiferroics of spin origin, *Rep. Prog. Phys.*, 2014, **77**, 076501.
9 P. Mandal, M. J. Pitcher, J. Alaria, H. Niu, P. Borisov, P. Stamenov, J. B. Claridge and M. J. Rosseinsky, Designing switchable polarization and magnetization at room temperature in an oxide, *Nature*, 2015, **525**, 363–367.
10 L. F. Henrichs, O. Cespedes, J. Bennett, j. Landers, S. Salamon, C. Heuser, T. Hansen, T. Helbig, O. Gutfleisch, D. C. Lupascu, H. Wende, W. Kleemann and A. J. Bell, Multiferroic clusters: A new perspective for relaxor-type room-temperature multiferroics, *Adv. Funct. Mater.*, 2016, **26**, 2111–2121.
11 C. M. Fernández-Posada, A. Castro, J. M. Kiat, F. Porcher, O. Peña, M. Algueró and H. Amorín, A novel perovskite oxide chemically designed to show multiferroic phase boundary with room-temperature magnetoelectricity, *Nat. Commun.*, 2016, **7**, 12772.
12 B. Aurivillius, Mixed bismuth oxides with layer lattices: 1. The structure type of $CaNb_2Bi_2O_9$, *Ark. Kemi*, 1950, **1**, 463–480.
13 B. Aurivillius, Mixed bismuth oxides with layer lattices: 2. Structure of $Bi_4Ti_3O_{12}$, *Ark. Kemi*, 1950, **1**, 499–512.
14 P. Millan, A. Castro and J. B. Torrance, The 1st doping of lead(2+) into the bismuth oxide layers of the Aurivillius oxides, *Mater. Res. Bull.*, 1993, **28**, 117–122.
15 A. Ramirez, R. Enjalbert, J. M. Rojo and A. Castro, New Aurivillius-related phases in the Sb-(W,V)-O system: Structural study and properties, *J. Solid State Chem.*, 1997, **128**, 30–37.
16 P. Durán-Martín, A. Castro, P. Millan and B. Jiménez, Influence of Bi-site substitution on the ferroelectricity of the Aurivillius compound $Bi_2SrNb_2O_9$, *J. Mater. Res.*, 1998, **13**, 2565–2571.
17 E. C. Subbarao, Crystal chemistry of mixed bismuth oxides with layer-type structure, *J. Am. Ceram. Soc.*, 1962, **45**, 166–169.
18 B. H. Park, B. S. Kang, S. D. Bu, T. W. Noh, J. Lee and W. Jo, Lanthanum-substituted bismuth titanate for use in non-volatile memories, *Nature*, 1999, **401**, 682–684.
19 H. X. Yan, H. T. Zhang, R. Ubic, M. J. Reece, J. Liu, Z. J. Shen and Z. Zhang, A lead-free high-Curie-point ferroelectric ceramic, $CaBi_2Nb_2O_9$, *Adv. Mater.*, 2005, **17**, 1261–1265.
20 X. Mao, W. Wang, X. Chen and Y. Lu, Multiferroic properties of layer-structured $Bi_5Fe_{0.5}Co_{0.5}Ti_3O_{15}$, *Appl. Phys. Lett.*, 2009, **95**, 082901.
21 L. Keeney, T. Maity, M. Schmidt, A. Amann, N. Deepak, N. Petkov, S. Roy, M. E. Pemble and R. W. Whatmore, Magnetic field-induced ferroelectric switching in multiferroic Aurivillius phase thin films at room temperature, *J. Am. Ceram. Soc.*, 2013, **96**, 2339–2357.
22 Z. Li, J. Ma, Z. P. Gao, G. Viola, V. Koval, A. Mahajan, X. Li, C. L. Jia, C. W. Nan and H. X. Yan, Room temperature magnetoelectric coupling in intrinsic multiferroic Aurivillius phase textured ceramics, *Dalton Trans.*, 2016, **45**, 14049–14052.
23 Z. Li, K. Tao, J. Ma, Z. P. Gao, V. Koval, C. J. Jiang, G. Viola, H. F. Zhang, A. Mahajan, J. Cao, M. Cain, I. Abrahams, C. W. Nan, C. L. Jia and H. X. Yan, $Bi_{3.25}La_{0.75}Ti_{3-2x}Nb_x(Fe_{0.5}Co_{0.5})_xO_{12}$, a single phase room temperature multiferroic, *J. Mater. Chem. C*, 2018, **6**, 2733–2740.
24 M. Algueró, M. Pérez-Cerdán, R. P. del Real, J. Ricote and A. Castro, $Bi_4Ti_{3-2x}Nb_xFe_xO_{12}$ phases with increasing magnetic-cation fraction until percolation: a novel approach for room temperature multiferroism, *J. Mater. Chem. C*, 2020, **8**, 12457–12469.
25 W. Bai, C. Chen, J. Yang, Y. Zhang, R. Qi, R. Huang, X. Tang, C. G. Duan and J. Chu, Dielectric behaviours of Aurivillius $Bi_5Ti_3Fe_{0.5}Cr_{0.5}O_{15}$multiferroic polycrystals: Detemining the intrinsic magnetoelectric responses by impedance spectroscopy, *Sci. Rep.*, 2015, **5**, 17846.
26 A. Srinivas, S. V. Suryanarayana, G. S. Kumar and M. M. Kumar, Magnetoelectric measurements on

$Bi_5FeTi_3O_{15}$ and $Bi_6Fe_2Ti_3O_{18}$, *J. Phys.: Condens. Matter*, 1999, **11**, 3335–3340.

27 A. Y. Birenbaum, A. Scaramucci and C. Ederer, Magnetic order in four-layered Aurivillius phases, *Phys. Rev. B*, 2017, **95**, 104419.

28 L. Kurzawski and K. Malarz, Simple cubic random-site percolation thresholds for complex neighbourhoods, *Rep. Math. Phys.*, 2012, **70**, 163–169.

29 A. Srinivas, M. M. Kumar, S. V. Suryanarayana and T. Bhimasankaram, Investigation of dielectric and magnetic nature of $Bi_7Fe_3Ti_3O_{21}$, *Mater. Res. Bull.*, 1999, **34**, 989–996.

30 A. Srinivas, D. W. Kim, K. S. Hong and S. V. Suryanarayana, Study of magnetic and magnetoelectric measurements in bismuth iron titanate ceramic $Bi_8Fe_4Ti_3O_{24}$, *Mater. Res. Bull.*, 2004, **39**, 55–61.

31 N. A. Lomanova, M. I. Morozov, V. L. Ugolkov and V. V. Gusarov, Properties of Aurivillius phases in the $Bi_4Ti_3O_{12}$- Bi_3FeO_3 system, *Inorg. Mater.*, 2006, **42**, 189–195.

32 W. Gu, X. Li, S. Sun, L. Zhu, Z. Fu and Y. Lu, Magnetocrystalline anisotropy in the Co/Fe codoped Aurivillius oxide with different perovskite layer number, *J. Am. Ceram. Soc.*, 2018, **101**, 2417–2427.

33 H. Zhao, H. Kimura, Z. Cheng, M. Osada, J. Wang, X. Wang, S. Dou, Y. Liu, J. Yu, T. Matsumoto, T. Tohei, N. Shibata and Y. Ikuhara, Large magnetoelectric coupling in magnetically short-range ordered $Bi_5Ti_3FeO_{15}$ film, *Sci. Rep.*, 2014, **4**, 5255.

34 M. Palizdar, T. P. Comyn, M. B. Ward, A. P. Brown, J. P. Harrington, S. Kulkarni, L. Keeney, S. Roy, M. Pemble, R. W. Whatmore, C. Quinn, S. H. Kilcoyne and A. J. Bell, Crystallographic and magnetic identification of secondary phase in orientated $Bi_5Fe_{0.5}Co_{0.5}Ti_3O_{15}$ ceramics, *J. Appl. Phys.*, 2012, **112**, 073919.

35 M. Tripathy, R. Mani and J. Gopalakrishnan, New Substitutions and novel derivatives of the Aurivillius phases $Bi_5TiNbWO_{15}$ and $Bi_4Ti_3O_{12}$, *Mater. Res. Bull.*, 2007, **42**, 950–960.

36 V. Koval, Y. Shi, I. Skorvanek, G. Viola, R. Bures, K. Saksl, P. Roupcova, M. Zhang, Ch. Jia and H. Yan, Cobalt-induced structural modulation in multiferroic Aurivillius-phase oxides, *J. Mater. Chem. C*, 2020, **8**, 8466–8483.

37 Z. Li, V. Koval, A. Mahajan, Z. Cao, C. Vecchini, M. Stewart, M. G. Cain, K. Tao, C. Jia, G. Viola and H. Yan, Room-temperature multiferroic behavior in layer-structured Aurivillius phase ceramics, *Appl. Phys. Lett.*, 2020, **117**, 052903.

38 M. A. Zurbuchen, R. S. Freitas, M. J. Wilson, P. Schiffer, M. Roeckerath, J. Schubert, M. D. Biegalski, G. H. Mehta, D. J. Comstock, J. H. Lee, Y. Jia and D. G. Schlom, Synthesis and characterization of an n = 6 Aurivillius phase incorporating magnetically active manganese, $Bi_7(Mn, Ti)_6O_{21}$, *Appl. Phys. Lett.*, 2007, **91**, 033113.

39 R. D. Shannon, Revised effective ionic radii and systematic studies of interatomic distances in halides and chalcogenides, *Acta Crystallogr., Sect. A: Cryst. Phys., Diffr., Theor. Gen. Crystallogr.*, 1976, **32**, 751–767.

40 R. A. Armstrong and R. E. Newnham, Bismuth titanate solid solutions, *Mater. Res. Bull.*, 1972, **7**, 1025–1034.

41 E. E. McCabe and C. Greaves, Structural and magnetic characterizations of $Bi_2Sr_{1.4}La_{0.6}Nb_2MnO_{12}$ and its relationship to "$Bi_2Sr_2Nb_2MnO_{12}$", *J. Mater. Chem.*, 2005, **15**, 177–182.

42 A. Gruverman, O. Auciello and H. Tokumoto, Imaging and control of domain structures in ferroelectric thin films via scanning force microscopy, *Annu. Rev. Mater. Sci.*, 1998, **28**, 101–123.

43 N. Salazar, M. Algueró, H. Amorín, A. Castro, A. Gil and J. Ricote, Local characterization of nanostructured high sensitivity piezoelectric $BiScO_3$-$PbTiO_3$ ceramics by piezoresponse force microscopy, *J. Appl. Phys.*, 2014, **116**, 124108.

44 R. Newnam, R. Wolfe and J. Dorrian, Structural basis of ferroelectricity in the bismuth titanate family, *Mater. Res. Bull.*, 1971, **6**, 1029–1040.

45 A. D. Rae, J. G. Thompson, R. L. Whiters and A. C. Willis, Structure refinement of commensurately modulated bismuth titanate $Bi_4Ti_3O_{12}$, *Acta Crystallogr., Sect. B: Struct. Sci.*, 1990, **46**, 474–487.

46 L. B. Kong, T. S. Zhang, J. Ma and F. Boey, Progress in synthesis of ferroelectric ceramic materials via high-energy mechanochemical technique, *Prog. Mater. Sci.*, 2008, **53**, 207–322.

47 M. Algueró, J. Ricote and A. Castro, Mechanosynthesis and thermal stability of piezoelectric perovskite 0.92Pb$(Zn_{1/3}Nb_{2/3})O_3$-$0.08PbTiO_3$ powders, *J. Am. Ceram. Soc.*, 2004, **87**, 772–778.

48 M. Algueró, J. Ricote, T. Hungria and A. Castro, High-sensitivity piezoelectric, low-tolerance-factor perovskites by mechanosynthesis, *Chem. Mater.*, 2007, **19**, 4982–4990.

49 A. Castro, C. Correas, O. Peña, A. R. Landa-Cánovas, M. Algueró, H. Amorín, M. Dollé, E. Vila and T. Hungría, Nanostructured $BiMnO_{3+\delta}$ obtained at ambient pressure: Analysis of its multiferroicity, *J. Mater. Chem.*, 2012, **22**, 9928–9938.

50 T. Hungria, H. Amorin, J. Galy, J. Ricote, M. Alguero and A. Castro, Nanostructured ceramics of 0.92PbZ$n_{1/3}Nb_{2/3}O_3$-$0.08PbTiO_3$ processed by SPS of nanocrystalline powders obtained by mechanosynthesis, *Nanotechnology*, 2008, **19**, 155609.

51 T. Hungría, H. Amorin, M. Algueró and A. Castro, Nanostructured ceramics of $BiScO_3$-$PbTiO_3$ with tailored grain size by spark plasma sintering, *Scr. Mater.*, 2011, **64**, 97–100.

52 J. A. Quintana-Cilleruelo, A. Castro, H. Amorín, V. K. Veerapandiyan, M. Deluca, O. Peña and M. Algueró, Ceramic processing and multiferroic properties of the perovskite $YMnO_3$-$BiFeO_3$ binary system, *J. Am. Ceram. Soc.*, 2020, **103**, 4846–4858.

53 A. Fouskova and L. E. Cross, Dielectric properties of bismuth titanate, *J. Appl. Phys.*, 1970, **41**, 2834–2838.

54 M. Takahashi, Y. Noguchi and M. Miyayama, Electrical conduction mechanism in $Bi_4Ti_3O_{12}$ single crystal, *Jpn. J. Appl. Phys.*, 2002, **41**, 7053–7056.

55 H. S. Shulman, D. Damjanovic and N. Setter, Niobium doping and dielectric anomalies in bismuth titanate, *J. Am. Ceram. Soc.*, 2000, **83**, 528–532.
56 M. Takahashi, Y. Noguchi and M. Miyayama, Estimation of ionic and hole conductivity in bismuth titanate polycrystals at high temperatures, *Solid State Ionics*, 2004, **172**, 325–329.
57 C. Elissalde and J. Ravez, Ferroelectric ceramics: Defects and dielectric relaxations, *J. Mater. Chem.*, 2001, **11**, 1957–1967.
58 P. Bintachitt, S. Jesse, D. Damjanovic, Y. Han, I. M. Reaney, S. Trolier-McKinstry and S. V. Kalinin, Collective dynamics underpins Rayleigh behavior in disordered polycrystalline ferroelectrics, *Proc. Natl. Acad. Sci. U. S. A.*, 2010, **107**, 7219–7224.
59 L. Keeney, C. Downing, M. Schmidt, M. E. Pemble, V. Nicolosi and R. W. Whatmore, Direct atomic scale determination of magnetic ion partition in a room temperature multiferroic material, *Sci. Rep.*, 2017, **7**, 1737.